Adaptive Lyapunov Function Method for Power System Transient Stability Analysis

Zitian Qiu, *Student Member, IEEE,* Chao Duan, *Member, IEEE,* Wei Yao, *Senior Member, IEEE,* Pingliang Zeng, *Senior Member, IEEE,* Lin Jiang, *Member, IEEE*

***Abstract*—Transient stability analysis is a crucial tool for evaluating the stability and ensuring the safe operation of power systems. Among existing methodologies for transient stability analysis, direct methods show merits in performing fast contingency screening and providing quantitative information for the degree of stability. However, the inherent conservatism of direct methods and their restriction on power system models still pose significant challenges for practical applications. This paper is devoted to further developing direct methods by proposing a novel *adaptive Lyapunov function method*, which enables simulation-free estimation of critical clearing time with drastically reduced conservatism. The novelties of the proposed method lie in three aspects. First, we propose an *adaptive sector condition* which bounds the nonlinearity of the power system model in an adjustable neighborhood of a given equilibrium. Second, we introduce an improved bounding technique for the time derivative of the Lyapunov function. Third, by exploiting the freedom of the adaptive sector condition and the *adjustable neighborhood*, the construction of Lyapunov functions along with the choice of the parameters in the sector conditions can be co-optimized to achieve the tightest possible estimation of the critical clearing time. The effectiveness of the proposed method is validated on four benchmark systems.**

***Index Terms*—Transient stability, direct method, adaptive Lyapunov function, critical clearing time, semi-definite program**

I. Introduction

TRANSIENT stability analysis (TSA) is one of the key tools to ensure the stable operation of power systems [1]–[3]. In normal conditions, a power system operates at a stable equilibrium point (SEP) determined by load distribution and generator dispatch. However, the normal operation is always at the risk of being challenged by sporadic faults. Once a fault occurs, the pre-fault equilibrium is no longer an SEP of the electromechanical dynamics and the system goes into transient. This fault-on transient process continues until the fault is cleared, after which a post-fault SEP, either identical or different from the pre-fault one, re-emerges. The system may be able to converge to the post-fault SEP and return to normal operation, or it may fail to do so and trigger the desynchronization among generators, which can result in system degradation and large-scale blackouts. To avoid these undesirable consequences and ensure system robustness against possible faults, power system TSA thus aims at determining the transient stability of the system, i.e., whether or not it can safely converge to the post-fault SEP given the information about pre-fault SEP, fault type and parameter, and fault clearing time (the time between the fault is initiated and cleared). The system is allowed to operate at a given SEP only when the system is declared to be transiently stable with this SEP under any faults in a pre-defined contingency set. The results of TSA can also guide the configuration of protective relay to ensure small enough clearing time under any faults in the contingency set. Due to its crucial role in power system operation, developing effective methods for TSA has been one of a central research topic for decades [3]–[5].

A straightforward approach to assess the transient stability of power systems is the time-domain simulation of the power system dynamics [6]–[9]. With the advantage of almost having no restriction on the complexity of the system model, time-domain simulation is widely adopted by the system operators as the main tool for power system TSA. Once the system model is correctly given, accurate conclusions about the transient stability of the system at a given operation point followed by any contingency can be visually drawn from the simulation curves. However, the time-domain simulation also comes with drawbacks. First, screening all possible contingencies on a regular basis is expensive even for off-line calculation and is prohibitive for on-line application. In fact, in practical power systems, most of the faults correspond to failures of relatively small and insignificant components, whose post-fault dynamics are close to the SEP and are therefore transiently stable [10]. Performing simulations for a huge amount of non-severe faults is unnecessary. Second, the time-domain simulation approach generally cannot reveal quantitative information on system stability margin and provide systematic guidance for the design of control and protection systems.

Complementary to the time-domain simulation is the direct methods which build on certain theoretical characterization of power system stability regions and avoid numerical integration as much as possible. Through energy interpretation or topological characterization of the region of stability, direct methods offer mechanistic understanding and quantitative information for transient stability, which can be useful to guide system operation and control design. Direct methods with different theoretical foundations have been applied to practical power systems as a valid tool for contingency screening [11]–[13]. Generally, the direct methods can be classified into three

Z. Qiu and L. Jiang are with the Department of Electrical Engineering and Electronics, University of Liverpool, Liverpool, L69 3GJ, UK (E-mail: zitian.qiu@liverpool.ac.uk, ljiang@liv.ac.uk).

C. Duan is with the Department of Physics and Astronomy, Northwestern University, Evanston, IL 60208, USA (E-mail: chao.duan@northwestern.edu).

W. Yao is with State Key Laboratory of Advanced Electromagnetic Engineering and Technology, School of Electrical and Electronic Engineering, Huazhong University of Science and Technology, Wuhan, 430074, China (E-mail: w.yao@hust.edu.cn).

P. Zeng is with the School of Automation, Hangzhou Dianzi University, Hangzhou, 310018, China (E-mail: plzeng@hotmail.com).

groups according to their underlying theories and methodologies. The first group of methods are based on the equal area criterion (EAC) [3] which is the well-known analytical results for power system transient stability on the single-machine-infinite-bus (SMIB) system, or equivalently, two-machine systems. System equivalence or approximation is needed to extend the EAC to multi-machine systems. In particular, the extended EAC (EEAC) method [14] decomposes the generators into two groups, each of which is dynamically approximated by an equivalent generator so that the EAC can be applied. The accuracy of the EEAC method depends critically on the correctness of grouping. To make an accurate prediction for the separation among generators, numerical integration of the fault-on or even the post-fault dynamics are employed in some form, which makes the EEAC method a hybrid integral-direct method [15]–[20].

The second group of direct methods rely on the construction of global energy function $V(\boldsymbol{x})$ and the associated topological characterization of stability regions [1], [21]–[24]. When a global energy function exists for the employed power system model, the stability boundary of any SEP is formed by the union of the stable manifolds of nearby unstable equilibrium points (UEPs). Hence, the level set $\{V(\boldsymbol{x}) \leq \rho\}$ with the critical energy value ρ given by the closest UEP constitutes an inner approximation of the stability region. This group of direct methods still require numerical integration of the fault-on dynamics to determine the fault-cleared state $\boldsymbol{x}_{cl}$ and then the transient stability of the system is determined by comparing $V(\boldsymbol{x}_{cl})$ and the critical energy value ρ. To reduce the conservative of this method, enormous effort has been devoted to developing more informed ways to determine the critical energy value ρ by further incorporating the trajectory information, which leads to techniques such as the potential energy surface (PES) method and the controlling UEP method. In addition, the boundary-controlling UEP (BCU) method [13] is an efficient numerical technique to compute the controlling UEP. However, the assumption on the existence of a global energy function poses a strong limitation on the power system models employed and creates inconsistency with industrial standards. Moreover, this group of methods still require the numerical integration of the fault-on or even the post-fault dynamics.

The third group of direct methods is the local Lyapunov function (LLF) method [10], [25]–[28] which seeks to construct a Lyapunov function $V(\boldsymbol{x})$ in a neighbour of a given (post-fault) SEP. Similar to the global energy function approach, the level set $\{V(\boldsymbol{x}) \leq \rho\}$ for some critical value ρ can be served as an inner approximation to the stability region. Different from the global energy function method, the critical function value ρ in the LLF method is not determined by nearby UEPs. Instead, the critical value ρ is chosen to ensure that the level set $\{V(\boldsymbol{x}) \leq \rho\}$ is an invariant set of the post-fault dynamics. With the theoretical and methodological advances in convex optimization, computational tools for constructing local Lyapunov functions and estimating the stability regions become available [27], [29], which stimulates recent revival of this classic idea applied to power system TSA [27], [30]. One prominent feature of the LLF method is that it is possible to completely avoid numerical integration by properly bounding the time derivative of the Lyapunov function along the fault-on trajectory [26], which makes this group of methods more consistent with the original motivation of a "direct method". In addition, the existence of a local Lyapunov function is always ensured by the converse Lyapunov function theorem [31], so that it does not impose any restriction on the power system model. However, the three major components of the LLF methods, i.e., certifying the Lyapunov conditions on $V(\boldsymbol{x})$, establishing the invariance of level set $\{V(\boldsymbol{x}) \leq \rho\}$, and bounding the time derivative of $V(\boldsymbol{x})$, all can introduce excessively high degree of conservatism, which makes the current LLF methods of limited practical value.

In light of the limitations of the state-of-the-art approaches, this paper further develops computational tools for power system TSA based on local Lyapunov functions by introducing several novel ideas that significantly reduce conservatism. Relative to existing LLF methods [10], [25]–[27], our novelties and contributions are four-fold:

1) The concepts of adjustable neighborhoods of equilibria and adaptive sector bounds for nonlinearities are introduced to reduce the conservatism originated from the certifying the Lyapunov conditions and the invariance of Lyapunov function level sets.
2) An improved bounding technique for the time derivative of Lyapunov functions is proposed to significantly reduce the conservatism coming from estimating the critical value of the Lyapunov functions.
3) A problem formulation and its solution method are developed to co-optimize and simultaneously determine the optimal estimation of the critical clearing time (CCT) along with the construction of Lyapunov functions and the adjustable neighborhoods of the post-fault equilibrium.
4) The proposed analysis approach can provide a systematic and optimization-based guide for control design, for which we exemplify in the context of virtual inertia and damping optimization for transient stability enhancement.

Due to the fact that the Lyapunov function, the adjustable neighborhood for certifying the Lyapunov conditions, and the sector conditions for nonlinearities are all chosen *adaptively* w.r.t. the system operation points and contingencies, we thus refer to our new method as the *adaptive Lyapunov function (ALF) method*. To validate the proposed ALF method, numerical studies are carried out on four benchmark systems in comparison to previous direct methods and time-domain simulations.

II. General framework of adaptive Lyapunov function method

Before diving into the technicalities of power systems, we present an abstract problem setup and outline a general framework of what we mean by the ALF method for TSA.

A. Problem setup and general framework

Consider a nonlinear system

$$\dot{\boldsymbol{x}} = \boldsymbol{A}\boldsymbol{x} + \boldsymbol{B}\boldsymbol{\phi}(\boldsymbol{C}\boldsymbol{x}), \tag{1}$$

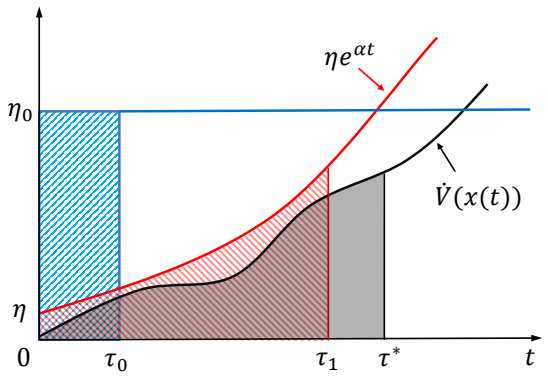

Fig. 1. Uniform (blue horizontal line) and non-uniform (red curve, assuming $V_0 = 0$) upper bounds for the time derivative of the Lyapunov function. For each bounding curve of $\dot{V}(\boldsymbol{x}(t))$, the corresponding CCT estimation is the time to which from $t = 0$ the integral of the bounding curve (the area under the curve) reaches a given critical Lyapunov function value ρ. Here, the estimated CCTs corresponding to uniform and non-uniform bounds are respectively given by τ_0 and τ_1 with comparison to the exact CCT τ^*.

where $\boldsymbol{x} \in \mathbb{R}^n$ is the state vector; $\boldsymbol{A} \in \mathbb{R}^{n\times n}$ represents the linear part of the system dynamics; $\boldsymbol{\phi}(\cdot) \in \mathbb{R}^l$ is a nonlinear function capturing all the system nonlinearity; $\boldsymbol{B} \in \mathbb{R}^{n\times l}$ and $\boldsymbol{C} \in \mathbb{R}^{p\times n}$ encode the coupling between nonlinearity and system states. Without loss of generality, it is assumed that $\boldsymbol{x} = \boldsymbol{0}$ is the equilibrium of system (1) relevant to our engineering applications. We are interested in the stability of the equilibrium under transient structural changes. That is, assume that the system stays at the equilibrium $\boldsymbol{x}(t) = \boldsymbol{0}$ for $t \le 0$; starting from $t = 0$, the system encounters a structural change (e.g., a fault) that forces the matrix $\boldsymbol{B}$ to be switched to a different matrix $\boldsymbol{B'}$ and hence brings the system state into transient. The incidence concludes (e.g., the fault is cleared) and the matrix $\boldsymbol{B'}$ is switched back to $\boldsymbol{B}$ at $t = \tau$. TSA deals with the question that whether the system state will return to the equilibrium $\boldsymbol{x} = \boldsymbol{0}$ after the transient and how the stability depends on the clearing time τ. The maximum clearing time τ_m under which the system remains stable is called the CCT.

The ALF method seeks to establish a rigorous mathematical characterization for any $\tau \le \tau_m$ given system information $(\boldsymbol{A}, \boldsymbol{B}, \boldsymbol{B'}, \boldsymbol{C}, \boldsymbol{\phi}(\cdot))$, which further leads to an algorithm to compute the CCT. To this end, we first construct a parametric set $\Omega(\boldsymbol{\gamma}) \subseteq \mathbb{R}^n$ which serves as a neighborhood of the equilibrium $\boldsymbol{x} = \boldsymbol{0}$. The size of the neighborhood $\Omega(\boldsymbol{\gamma})$ is tunable by changing the parameter $\boldsymbol{\gamma}$. Based on $\Omega(\boldsymbol{\gamma})$, we can construct a local Lyapunov function $V(\boldsymbol{x})$ of system (1), i.e.,

$$V(\boldsymbol{0}) = 0,\ V(\boldsymbol{x}) > 0,\ \dot{V}(\boldsymbol{x}) < 0,\ \forall \boldsymbol{x} \in \Omega(\boldsymbol{\gamma})/\{\boldsymbol{0}\}. \quad (2)$$

Further exploiting the information of $\Omega(\boldsymbol{\gamma})$ and the structural change $\boldsymbol{B'}$, we derive an upper bound for the time derivative of the Lyapunov function in the form

$$\dot{V}(\boldsymbol{x}) \le \eta + \alpha V(\boldsymbol{x}),\ \forall \boldsymbol{x} \in \Omega(\boldsymbol{\gamma}), \quad (3)$$

during the period of the structural change. When inequality (3) holds for some parameters η and α, due to the comparison principle [31, p.126], we obtain

$$V(\boldsymbol{x}(t)) \le e^{\alpha t} V_0 + \frac{\eta}{\alpha}(e^{\alpha t} - 1), \quad (4)$$

where $V_0 = V(\boldsymbol{x}(0))$. When the pre-fault equilibrium is identical to the post-fault equilibrium, we have $V_0 = 0$. In this paper, if not mentioned otherwise, we always assume that $V_0 = 0$ for simplicity though our theory framework can be straightforwardly extended to the case where the post-fault equilibrium differs from the pre-fault equilibrium (hence $V_0 \neq 0$). Further note that, given a Lyapunov function $V(\boldsymbol{x})$, any level set inside the neighborhood $\Omega(\boldsymbol{\gamma})$, i.e.,

$$\{V(\boldsymbol{x}) \le \rho\} \subseteq \Omega(\boldsymbol{\gamma}), \quad (5)$$

is a subset of the domain of attraction for the equilibrium $x = 0$. Therefore, a clearing time τ is less than τ_m if

$$\frac{\eta}{\alpha}(e^{\alpha\tau} - 1) \le \rho, \quad (6)$$

which implies that $\frac{1}{\alpha}\ln(\frac{\alpha\rho+\eta}{\eta})$ is a lower approximation of the critical clearing time τ_m. It is worth noting that, in stark contrast to recent works [10], [26], where a uniform bound is employed for the time derivative of the Lyapunov function, we introduce a non-uniform bound in Eq. (3) for $\dot{V}(\boldsymbol{x})$, which results in tighter bounds for the value of the Lyapunov function during the fault-on dynamics. As illustrated in Fig. 1, the tighter bounds lead to less conservative CCT estimation given the same critical Lyapunov function value ρ.

To approximate τ_m as tight as possible, theoretically speaking, we can solve the following problem

$$\max_{V(\cdot)\in\mathcal{C}(\mathbb{R}^n),\boldsymbol{\gamma},\rho,\eta,\alpha} \ \frac{1}{\alpha}\ln(\frac{\alpha\rho+\eta}{\eta}),\ \text{s.t. } (2),(3),(5), \quad (7)$$

where $\mathcal{C}(\mathbb{R}^n)$ is the space of continuous functions on $\mathbb{R}^n$. The problem seeks to find the optimal Lyapunov function $V(\cdot)$, adjustable neighborhood parameter $\boldsymbol{\gamma}$, the level set parameter ρ, and the time derivative bounding parameters η and α that together achieve the least conservative estimation of the CCT τ_m. In stark contrast to previous Lyapunov function methods, in the proposed formulation (7), not only the Lyapunov function $V(\cdot)$ but also the bounding neighborhood $\Omega(\boldsymbol{\gamma})$ are adaptive to the information of the particular system and structural change, and the construction of the Lyapunov function and the estimation of the CCT is done simultaneously. For this reason, we call the proposed solution framework the ALF method. By properly parameterizing the Lyapunov function $V(\cdot)$ and reformulating the constraints (2)-(3), the problem (7) can be cast into a finite-dimensional convex optimization problem which is solvable by off-the-shelf solvers.

B. Quadratic Lyapunov Function

Here, we specialize the above general framework to the simple yet powerful quadratic Lyapunov function. That is, we parametrize the candidate Lyapunov function as $V(\boldsymbol{x}) = \boldsymbol{x}^{\mathrm{T}}\boldsymbol{P}\boldsymbol{x}$ for some matrix $\boldsymbol{P} \in \mathbb{S}^n$, where $\mathbb{S}^n$ denotes the set of $n \times n$ real symmetric matrices.

In addition, by properly designing the structure of the neighborhood $\Omega(\boldsymbol{\gamma})$, it facilitates the local bounding of the system nonlinearity. That is, there exist two parametric ma-

$$\boldsymbol{P}\geq 0,\ \begin{bmatrix}\boldsymbol{A}^{\mathrm{T}}\boldsymbol{P}+\boldsymbol{P}\boldsymbol{A}-\alpha\boldsymbol{P}-\boldsymbol{C}^{\mathrm{T}}\boldsymbol{G}(\boldsymbol{\gamma})\boldsymbol{C} & \boldsymbol{P}\boldsymbol{B}+\boldsymbol{C}^{\mathrm{T}}\boldsymbol{H}(\boldsymbol{\gamma})^{\mathrm{T}}\mathrm{diag}(\boldsymbol{\lambda}) & \boldsymbol{P}\boldsymbol{S}\\ \boldsymbol{B}^{\mathrm{T}}\boldsymbol{P}+\mathrm{diag}(\boldsymbol{\lambda})\boldsymbol{H}(\boldsymbol{\gamma})\boldsymbol{C} & -\mathrm{diag}(\boldsymbol{\lambda}) & \boldsymbol{0}_{n\times l}\\ \boldsymbol{S}^{\mathrm{T}}\boldsymbol{P} & \boldsymbol{0}_{l\times n} & -\eta\boldsymbol{I}_n\end{bmatrix}\leq\boldsymbol{0},\ \boldsymbol{\lambda}\geq\boldsymbol{0}, \tag{9}$$

trices $\boldsymbol{H'}(\boldsymbol{\gamma})\in\mathbb{R}^{l\times p}$ and $\boldsymbol{H''}(\boldsymbol{\gamma})\in\mathbb{R}^{l\times p}$ such that the following adaptive sector condition holds

$$\big(\boldsymbol{\phi}(\boldsymbol{C}\boldsymbol{x})-\boldsymbol{H'}(\boldsymbol{\gamma})\boldsymbol{C}\boldsymbol{x}\big)^{\mathrm{T}}\boldsymbol{E}_k\big(\boldsymbol{\phi}(\boldsymbol{C}\boldsymbol{x})-\boldsymbol{H''}(\boldsymbol{\gamma})\boldsymbol{C}\boldsymbol{x}\big)\leq 0,\quad \forall\boldsymbol{x}\in\Omega(\boldsymbol{\gamma}),\ \forall 1\leq k\leq l, \tag{8}$$

where $\boldsymbol{E}_k$ denotes the matrix with the (k,k)th element being 1 and all other elements being 0. From an optimization perspective, condition (8) can be considered a robust constraint on the state $\boldsymbol{x}$ whose uncertainty set $\Omega(\boldsymbol{\gamma})$ is adjustable so that a desirable trade-off between conservatism and region of validness can be achieved by optimizing parameter $\boldsymbol{\gamma}$. Without loss of generality, we assume that the structural change takes the form $\boldsymbol{B'}=\boldsymbol{B}+\boldsymbol{S}\boldsymbol{\Delta}$, where $\boldsymbol{S}$ and $\boldsymbol{\Delta}$ are two matrices of appropriate dimensions and the matrix $\boldsymbol{\Delta}$ satisfies $\boldsymbol{\phi}^{\mathrm{T}}\boldsymbol{\Delta}^{\mathrm{T}}\boldsymbol{\Delta}\boldsymbol{\phi}\leq 1$. Using S-Lemma and Schur complement, the Lyapunov function condition (2), the bounding inequality (3), and the adaptive sector condition (8) hold simultaneously if the robust linear matrix inequality (9) is satisfied, in which

$$\boldsymbol{H}(\boldsymbol{\gamma})=\frac{\boldsymbol{H'}(\boldsymbol{\gamma})+\boldsymbol{H''}(\boldsymbol{\gamma})}{2}, \tag{10}$$

$$\boldsymbol{G}(\boldsymbol{\gamma})=\frac{\boldsymbol{H'}(\boldsymbol{\gamma})^{\mathrm{T}}\mathrm{diag}(\boldsymbol{\lambda})\boldsymbol{H''}(\boldsymbol{\gamma})+\boldsymbol{H''}(\boldsymbol{\gamma})^{\mathrm{T}}\mathrm{diag}(\boldsymbol{\lambda})\boldsymbol{H'}(\boldsymbol{\gamma})}{2}, \tag{11}$$

and $\boldsymbol{\lambda}=(\lambda_i)$, $1\leq i\leq l$, are the auxiliary variables introduced by S-Lemma.

To reformulate condition (5), we further assume that the parametric neighborhood $\Omega(\boldsymbol{\gamma})$ is a polyhedron of the form

$$\Omega(\boldsymbol{\gamma})=\{\boldsymbol{x}\in\mathbb{R}^n\mid \underline{\boldsymbol{b}}(\boldsymbol{\gamma})\leq\boldsymbol{C}\boldsymbol{x}\leq\overline{\boldsymbol{b}}(\boldsymbol{\gamma})\}, \tag{12}$$

where the lower bounds $\underline{\boldsymbol{b}}(\boldsymbol{\gamma})\in\mathbb{R}^p$ and upper bounds $\overline{\boldsymbol{b}}(\boldsymbol{\gamma})\in\mathbb{R}^p$ are linear functions of parameter $\boldsymbol{\gamma}$. By further using S-lemma, condition (5) holds if there exist auxiliary variables $\underline{\boldsymbol{\mu}}\in\mathbb{R}^p$ and $\overline{\boldsymbol{\mu}}\in\mathbb{R}^p$ such that

$$\underline{\boldsymbol{\mu}}\geq\boldsymbol{0},\ \begin{bmatrix}\boldsymbol{P} & \frac{1}{2}C^{\mathrm{T}}\boldsymbol{E}_k\underline{\boldsymbol{\mu}}\\ \frac{1}{2}\underline{\boldsymbol{\mu}}^{\mathrm{T}}\boldsymbol{E}_k\boldsymbol{C} & -\rho-\underline{\boldsymbol{\mu}}^{\mathrm{T}}\boldsymbol{E}_k\underline{\boldsymbol{b}}(\boldsymbol{\gamma})\end{bmatrix}\geq\boldsymbol{0},\forall 1\leq k\leq p, \tag{13a}$$

$$\overline{\boldsymbol{\mu}}\geq\boldsymbol{0},\ \begin{bmatrix}\boldsymbol{P} & -\frac{1}{2}\boldsymbol{C}^{\mathrm{T}}\boldsymbol{E}_k\overline{\boldsymbol{\mu}}\\ -\frac{1}{2}\overline{\boldsymbol{\mu}}^{\mathrm{T}}\boldsymbol{E}_k\boldsymbol{C} & -\rho+\overline{\boldsymbol{\mu}}^{\mathrm{T}}\boldsymbol{E}_k\overline{\boldsymbol{b}}(\boldsymbol{\gamma})\end{bmatrix}\geq\boldsymbol{0},\forall 1\leq k\leq p. \tag{13b}$$

Following above analysis, the functional optimization problem (7) can be cast into the following semi-definite program (SDP)

$$\max_{\boldsymbol{P}\in\mathbb{S}^n,\boldsymbol{\gamma},\rho,\eta,\boldsymbol{\lambda},\underline{\boldsymbol{\mu}},\overline{\boldsymbol{\mu}},\alpha}\ \rho\eta^{-1}\ \text{s.t. (9), (13).} \tag{14}$$

In the subsequent sections, we will specialize this general framework to power system TSA, for which we show that the nonlinear semi-definite program (14) can be solved by convex solvers.

III. Power System Transient Stability Analysis

Here, we show that the general method developed in the previous Section is readily applicable to power system TSA.

A. System model

To formulate the power system electrical-mechanical dynamics in the form of Eq. (1), we adopt the structure-preserving model [11], [32] in which the loads and the generators are represented by first- and second-order differential equations, respectively. Without loss of generality, we assume that the network has n_b buses in total, among which the first n_c buses are pure load consumption buses and the rest n_g ones are generator buses. Here, we have $n_b=n_c+n_g$. Let n_l be the number of transmission lines. We define a $n_l\times n_b$ matrix $\boldsymbol{F}$ whose (k,i)th element is 1 if the kth transmission line takes bus i as its "from" end. Similarly, we define a $n_l\times n_b$ matrix $\boldsymbol{T}$ whose (k,i)th element is 1 if the kth transmission line takes bus i as its "to" end. Other unspecified elements of $\boldsymbol{F}$ and $\boldsymbol{T}$ are all zeros. We also define $\bar{\boldsymbol{C}}=\boldsymbol{F}-\boldsymbol{T}$. For convenience, we use vector $\bar{\boldsymbol{c}}_k$ to denote the kth row of matrix $\bar{\boldsymbol{C}}$. We also use scalars f_{ki} and t_{ki} to denote the (k,i)th element of the matrices $\boldsymbol{F}$ and $\boldsymbol{T}$, respectively. In addition, the $n_l\times 1$ complex vector $\boldsymbol{y}$ represents the admittance of transmission lines, i.e., $y_k=|y_k|\angle\varphi_k$ is the admittance (with magnitude $|y_k|$ and phase φ_k) of the kth line. We also define a coupling strength vector $\boldsymbol{\sigma}\in\mathbb{R}^{n_l\times 1}$ with the kth element $\sigma_k=V_iV_j|y_k|$ where V_i and V_j are the voltage magnitudes of the "from" and "to" ends of the kth transmission line, respectively.

The power system dynamics are described by

$$r_i\dot{\delta}_i+\sum_{k=1}^{n_l}\sigma_k\big[f_{ki}\sin\left(\bar{\boldsymbol{c}}_k\boldsymbol{\delta}+\varphi_k\right)+t_{ki}\sin\left(-\bar{\boldsymbol{c}}_k\boldsymbol{\delta}+\varphi_k\right)\big]=-P_{di},i=1,2,\cdots,n_c, \tag{15a}$$

$$m_i\ddot{\delta}_i+d_i\dot{\delta}_i+\sum_{k=1}^{n_l}\sigma_k\big[f_{ki}\sin(\bar{\boldsymbol{c}}_k\boldsymbol{\delta}+\varphi_k)+t_{ki}\sin(-\bar{\boldsymbol{c}}_k\boldsymbol{\delta}+\varphi_k)\big]=P_{mi},i=n_c+1,n_c+2,\cdots,n_b, \tag{15b}$$

where m_i and d_i represent the inertia and damping coefficients of the generator at bus i with P_{mi} being its mechanical power input. The constant r_i is the frequency coefficient and P_{di} represents the power consumption of the load at bus i. In the steady state, the system operates at a given equilibrium $\boldsymbol{\delta}^*$ that satisfies the power flow equations

$$\sum_{k=1}^{n_l}\sigma_k\big[f_{ki}\sin\left(\bar{\boldsymbol{c}}_k\boldsymbol{\delta}^*+\varphi_k\right)+t_{ki}\sin\left(-\bar{\boldsymbol{c}}_k\boldsymbol{\delta}^*+\varphi_k\right)\big]=-P_{di},\quad i=1,2,\cdots,n_c, \tag{16a}$$

$$\sum_{k=1}^{n_l}\sigma_k\big[f_{ki}\sin(\bar{\boldsymbol{c}}_k\boldsymbol{\delta}^*+\varphi_k)+t_{ki}\sin(-\bar{\boldsymbol{c}}_k\boldsymbol{\delta}^*+\varphi_k)\big]=P_{mi},\quad i=n_c+1,n_c+2,\cdots,n_b. \tag{16b}$$

By subtracting Eq. (16) from Eq. (15) and re-defining state variables $\boldsymbol{x}=[\boldsymbol{x_1},\boldsymbol{x_2},\boldsymbol{x_3}]^{\mathrm{T}}$, where $\boldsymbol{x_1}=[\delta_1-\delta_1^*,\delta_2-$

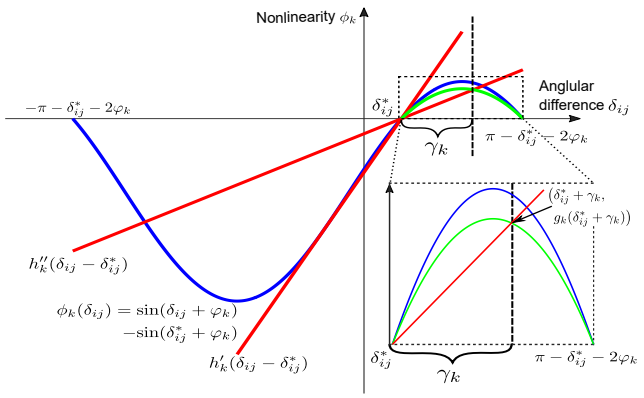

Fig. 2. Adaptive sector bounds for the nonlinearity corresponding to the transmission line k which collects bus i and bus j, whose $\delta^*_{ij} \geq 0$. The nonlinearity is shown as the blue sinusoidal curve, which is locally approximated by a quadratic function (in green) and bounded by two linear functions (in red).

$\delta^*_2, \cdots, \delta_{n_c} - \delta^*_{n_c}]$, $\boldsymbol{x_2} = [\delta_{n_c+1} - \delta^*_{n_c+1}, \cdots, \delta_{n_b} - \delta^*_{n_b}]$, and $\boldsymbol{x_3} = [\dot{\delta}_{n_c+1}, \cdots, \dot{\delta}_{n_b}]$, we can rewrite dynamical system (15) in the form of Eq. (1) with

$$\boldsymbol{A} = \begin{bmatrix} \boldsymbol{0}_{n_c \times n_c} & \boldsymbol{0}_{n_c \times n_g} & \boldsymbol{0}_{n_c \times n_g} \\ \boldsymbol{0}_{n_g \times n_c} & \boldsymbol{0}_{n_g \times n_g} & \boldsymbol{I}_{n_g} \\ \boldsymbol{0}_{n_g \times n_c} & \boldsymbol{0}_{n_g \times n_g} & -\boldsymbol{M}^{-1}\boldsymbol{D} \end{bmatrix}, \tag{17}$$

$$\boldsymbol{B} = \begin{bmatrix} \boldsymbol{R}^{-1} & \boldsymbol{0}_{n_c \times n_g} \\ \boldsymbol{0}_{n_g \times n_c} & \boldsymbol{0}_{n_g \times n_g} \\ \boldsymbol{0}_{n_g \times n_c} & \boldsymbol{M}^{-1} \end{bmatrix} \begin{bmatrix} -\boldsymbol{F}^{\mathrm{T}}\boldsymbol{\Sigma} & -\boldsymbol{T}^{\mathrm{T}}\boldsymbol{\Sigma} \end{bmatrix}, \tag{18}$$

$$\boldsymbol{C} = \begin{bmatrix} \bar{\boldsymbol{C}} & \boldsymbol{0}_{n_l \times n_g} \end{bmatrix} \tag{19}$$

$$\boldsymbol{\phi}(\boldsymbol{Cx}) = \begin{bmatrix} \sin\left(\bar{\boldsymbol{C}}\boldsymbol{\delta} + \boldsymbol{\varphi}\right) - \sin\left(\bar{\boldsymbol{C}}\boldsymbol{\delta}^* + \boldsymbol{\varphi}\right) \\ \sin\left(-\bar{\boldsymbol{C}}\boldsymbol{\delta} + \boldsymbol{\varphi}\right) - \sin\left(-\bar{\boldsymbol{C}}\boldsymbol{\delta}^* + \boldsymbol{\varphi}\right) \end{bmatrix}, \tag{20}$$

where diagonal matrices $\boldsymbol{D} = \mathrm{diag}(d_1, d_2, \cdots, d_{n_g})$, $\boldsymbol{M} = \mathrm{diag}(m_1, m_2, \cdots, m_{n_g})$, $\boldsymbol{R} = \mathrm{diag}(r_1, r_2, \cdots, r_{n_c})$, and $\boldsymbol{\Sigma} = \mathrm{diag}(\sigma_1, \sigma_2, \cdots, \sigma_{n_l})$. The $\sin(\cdot)$ function applies to the vector argument element-wisely.

We consider a symmetrical line-tripping fault of the kth transmission line. The fault is cleared and the line is successfully re-closed after a certain period of time. Following the framework developed in Section-II-B, the fault is modelled as the switching of matrix $\boldsymbol{B}$ to $\boldsymbol{B}' = \boldsymbol{B} + \boldsymbol{S}\boldsymbol{\Delta}$. Here,

$$\boldsymbol{S} = \begin{bmatrix} \boldsymbol{R}^{-1} & \boldsymbol{0}_{n_c \times n_g} \\ \boldsymbol{0}_{n_g \times n_c} & \boldsymbol{0}_{n_g \times n_g} \\ \boldsymbol{0}_{n_g \times n_c} & \boldsymbol{M}^{-1} \end{bmatrix} \begin{bmatrix} \boldsymbol{F}^{\mathrm{T}}\boldsymbol{\Sigma}\bar{\boldsymbol{E}}_k & \boldsymbol{T}^{\mathrm{T}}\boldsymbol{\Sigma}\bar{\boldsymbol{E}}_k \end{bmatrix}, \tag{21}$$

and $\boldsymbol{\Delta} = \boldsymbol{I}_{2n_l}$, where $\bar{\boldsymbol{E}}_k$ is the $n_l \times n_l$ matrix with its (k,k)th element being 1 and all other elements being zeros. Note that here we take the line tripping fault as an example to illustrate how the structure changes. The proposed approach can also be extended to short-circuit faults. The way to construct structure change matrix $\tilde{\boldsymbol{S}}$ accordingly is thoroughly given in Section-V-B.

B. Adaptive sector conditions for nonlinearity

The nonlinearity of the model defined by Eq. (1) and Eqs. (17)-(20) is entirely captured by the nonlinear function $\boldsymbol{\phi}(\boldsymbol{Cx})$. Here, we derive sector conditions for the nonlinear term $\boldsymbol{\phi}(\boldsymbol{Cx})$ by specifying the structures of the neighborhood $\Omega(\boldsymbol{\gamma})$ and the matrices $\boldsymbol{H'}(\boldsymbol{\gamma})$ and $\boldsymbol{H''}(\boldsymbol{\gamma})$.

Given the steady-state power flow solution $\boldsymbol{\delta}^*$, the neighborhood $\Omega(\boldsymbol{\gamma})$ is constructed as the following parametric polyhedron

$$\Omega(\boldsymbol{\gamma}) = \{\boldsymbol{x} \in \mathbb{R}^{n_c+2n_g} \;\big|\; -\boldsymbol{\gamma} \leq \boldsymbol{Cx} \leq \boldsymbol{\gamma}\}, \tag{22}$$

where $\boldsymbol{\gamma} \in \mathbb{R}^{n_l}$ is a non-negative vector whose kth element γ_k encodes the allowable deviation of the rotor angle difference $\delta_i - \delta_j$ from $\delta^*_i - \delta^*_j$, where bus i and bus j are the "from" and "to" ends of the kth transmission line, respectively. With this simple structure of $\Omega(\boldsymbol{\gamma})$, we can then derive sector bounds for the nonlinear term $\boldsymbol{\phi}(\boldsymbol{Cx})$ in Eq. (20). To achieve this, we first consider the kth element of $\boldsymbol{\phi}$, i.e.,

$$\phi_k(\bar{\boldsymbol{c}}_k\boldsymbol{\delta}) = \sin\left(\bar{\boldsymbol{c}}_k\boldsymbol{\delta} + \varphi_k\right) - \sin\left(\bar{\boldsymbol{c}}_k\boldsymbol{\delta}^* + \varphi_k\right) \tag{23}$$

for some $1 \leq k \leq n_l$. Within the neighborhood $\Omega(\boldsymbol{\gamma})$ defined in (22), $|\bar{\boldsymbol{c}}_k(\boldsymbol{\delta} - \boldsymbol{\delta}^*)| \leq \gamma_k$, we seek to find two parametric scalars h'_k and h''_k, possibly depending on γ_k, such that

$$\left(\phi_k - h'_k\bar{\boldsymbol{c}}_k(\boldsymbol{\delta} - \boldsymbol{\delta}^*)\right)\left(\phi_k - h''_k\bar{\boldsymbol{c}}_k(\boldsymbol{\delta} - \boldsymbol{\delta}^*)\right) \leq 0 \tag{24}$$

holds for all $\boldsymbol{\delta}$ that satisfies $|\bar{\boldsymbol{c}}_k(\boldsymbol{\delta} - \boldsymbol{\delta}^*)| \leq \gamma_k$.

The method to determine scalars h'_k and h''_k is illustrated in Fig. 2. We start the analysis by assuming that $\bar{\boldsymbol{c}}_k\boldsymbol{\delta}^* \geq 0$. In this case, on the $\bar{\boldsymbol{c}}_k\boldsymbol{\delta}$ v.s. ϕ_k plane, the scalar h'_k can be chosen as the slope of the line (the red line in Fig. 2) that crosses the equilibrium $\bar{\boldsymbol{c}}_k\boldsymbol{\delta}^*$ while being tangent to the graph of function $\phi_k(\bar{\boldsymbol{c}}_k\boldsymbol{\delta})$ (the blue sine curve in Fig. 2). The tangent point always lies in the orthant of $\phi_k \leq 0$ with x-coordinate z_k satisfying

$$\cos(z_k + \varphi_k) \cdot (z_k - \bar{\boldsymbol{c}}_k\boldsymbol{\delta}^*) = \sin(z_k + \varphi_k) - \sin(\bar{\boldsymbol{c}}_k\boldsymbol{\delta}^* + \varphi_k). \tag{25}$$

By solving the above equation, we obtain

$$h'_k(\bar{\boldsymbol{c}}_k\boldsymbol{\delta}^*) = \cos(z_k + \varphi_k). \tag{26}$$

With this choice of h'_k, we have $h'_k\bar{\boldsymbol{c}}_k(\boldsymbol{\delta} - \boldsymbol{\delta}^*) \geq \phi(\bar{\boldsymbol{c}}_k\boldsymbol{\delta})$ for $\bar{\boldsymbol{c}}_k\boldsymbol{\delta}^* \leq \bar{\boldsymbol{c}}_k\boldsymbol{\delta} \leq \bar{\boldsymbol{c}}_k\boldsymbol{\delta}^* + \gamma_k$, whereas $h'_k\bar{\boldsymbol{c}}_k(\boldsymbol{\delta} - \boldsymbol{\delta}^*) \leq \phi(\bar{\boldsymbol{c}}_k\boldsymbol{\delta})$ for $\bar{\boldsymbol{c}}_k\boldsymbol{\delta}^* - \gamma_k \leq \bar{\boldsymbol{c}}_k\boldsymbol{\delta} \leq \bar{\boldsymbol{c}}_k\boldsymbol{\delta}^*$.

To derive the scalar h''_k, we introduce a quadratic function that provides the tightest lower bound for the nonlinear function $\phi_k(\bar{\boldsymbol{c}}_k\boldsymbol{\delta})$ in the region of $\bar{\boldsymbol{c}}_k\boldsymbol{\delta} \geq \bar{\boldsymbol{c}}_k\boldsymbol{\delta}^*$, as illustrated by the green curve in Fig. 2. It is obvious that the quadratic function crosses the points $(\bar{\boldsymbol{c}}_k\boldsymbol{\delta}^*, 0)$ and $(\pi - \bar{\boldsymbol{c}}_k\boldsymbol{\delta}^* - 2\varphi_k, 0)$ thus taking the form

$$g_k(\bar{\boldsymbol{c}}_k\boldsymbol{\delta}) = -a_k\left(\bar{\boldsymbol{c}}_k\boldsymbol{\delta} - \bar{\boldsymbol{c}}_k\boldsymbol{\delta}^*\right)\left(\bar{\boldsymbol{c}}_k\boldsymbol{\delta} - (\pi - \bar{\boldsymbol{c}}_k\boldsymbol{\delta}^* - 2\varphi_k)\right) \tag{27}$$

for some scalar $a_k > 0$. In order for $g_k(\bar{\boldsymbol{c}}_k\boldsymbol{\delta})$ to be the tightest possible quadratic lower bound, the curve for $g_k(\bar{\boldsymbol{c}}_k\boldsymbol{\delta})$ must be tangent to that for the nonlinear function $\phi_k(\bar{\boldsymbol{c}}_k\boldsymbol{\delta})$ at the equilibrium point $(\bar{\boldsymbol{c}}_k\boldsymbol{\delta}^*, 0)$, leading to the following optimal choice of parameter

$$a_k = \frac{\cos(\bar{\boldsymbol{c}}_k\boldsymbol{\delta}^* + \varphi_k)}{\pi - 2\bar{\boldsymbol{c}}_k\boldsymbol{\delta}^* - 2\varphi_k}. \tag{28}$$

Due to the concavity of the function $g_k(\bar{\boldsymbol{c}}_k\boldsymbol{\delta})$, given any scalar $0 \le \gamma_k \le \pi - 2\bar{\boldsymbol{c}}_k\boldsymbol{\delta}^* - 2\varphi_k$, the secant that passes through $(\bar{\boldsymbol{c}}_k\boldsymbol{\delta}^*, 0)$ and $(\bar{\boldsymbol{c}}_k\boldsymbol{\delta}^* + \gamma_k, g_k(\bar{\boldsymbol{c}}_k\boldsymbol{\delta}^* + \gamma_k))$ also provide a lower bound for the function $\phi_k(\bar{\boldsymbol{c}}_k\boldsymbol{\delta})$ in the interval $\bar{\boldsymbol{c}}_k\boldsymbol{\delta}^* \le \bar{\boldsymbol{c}}_k\boldsymbol{\delta} \le \bar{\boldsymbol{c}}_k\boldsymbol{\delta}^* + \gamma_k$. See the inset of Fig. 2 for a clear illustration. Obviously, the same secant provides an upper bound for function $\phi_k(\bar{\boldsymbol{c}}_k\boldsymbol{\delta})$ in the interval $\bar{\boldsymbol{c}}_k\boldsymbol{\delta}^* - \gamma_k \le \bar{\boldsymbol{c}}_k\boldsymbol{\delta} \le \bar{\boldsymbol{c}}_k\boldsymbol{\delta}^*$. Therefore, by choosing h_k'' to be the slope of the secant, i.e.,

$$\begin{aligned} h_k''(\gamma_k, \bar{\boldsymbol{c}}_k\boldsymbol{\delta}^*) &= \frac{g_k(\bar{\boldsymbol{c}}_k\boldsymbol{\delta}^* + \gamma_k)}{\gamma_k} \\ &= \frac{\cos(\bar{\boldsymbol{c}}_k\boldsymbol{\delta}^* + \varphi_k)}{\pi - 2\bar{\boldsymbol{c}}_k\boldsymbol{\delta}^* - 2\varphi_k}(\pi - 2\bar{\boldsymbol{c}}_k\boldsymbol{\delta}^* - 2\varphi_k - \gamma_k), \end{aligned} \tag{29}$$

we have $h_k''(\gamma_k, \bar{\boldsymbol{c}}_k\boldsymbol{\delta}^*) \cdot (\bar{\boldsymbol{c}}_k\boldsymbol{\delta} - \bar{\boldsymbol{c}}_k\boldsymbol{\delta}^*) \le \phi(\bar{\boldsymbol{c}}_k\boldsymbol{\delta})$ for $\bar{\boldsymbol{c}}_k\boldsymbol{\delta}^* \le \bar{\boldsymbol{c}}_k\boldsymbol{\delta} \le \bar{\boldsymbol{c}}_k\boldsymbol{\delta}^* + \gamma_k$, whereas $h_k''(\gamma_k, \bar{\boldsymbol{c}}_k\boldsymbol{\delta}^*) \cdot (\bar{\boldsymbol{c}}_k\boldsymbol{\delta} - \bar{\boldsymbol{c}}_k\boldsymbol{\delta}^*) \ge \phi(\bar{\boldsymbol{c}}_k\boldsymbol{\delta})$ for $\bar{\boldsymbol{c}}_k\boldsymbol{\delta}^* - \gamma_k \le \bar{\boldsymbol{c}}_k\boldsymbol{\delta} \le \bar{\boldsymbol{c}}_k\boldsymbol{\delta}^*$. The above choices for h_k' and h_k'' ensure the sector condition (24) hold for all $\bar{\boldsymbol{c}}_k\boldsymbol{\delta}$ that satisfies $|\bar{\boldsymbol{c}}_k\boldsymbol{\delta} - \bar{\boldsymbol{c}}_k\boldsymbol{\delta}^*| \le \gamma_k$.

The above analysis extends analogously to the case where $\bar{\boldsymbol{c}}_k\boldsymbol{\delta}^* \le 0$. The only difference in this case is that

$$h_k''(\gamma_k, \bar{\boldsymbol{c}}_k\boldsymbol{\delta}^*) = \frac{\cos(\bar{\boldsymbol{c}}_k\boldsymbol{\delta}^* + \varphi_k)}{\pi + 2\bar{\boldsymbol{c}}_k\boldsymbol{\delta}^* + 2\varphi_k}(\pi + 2\bar{\boldsymbol{c}}_k\boldsymbol{\delta}^* + 2\varphi_k - \gamma_k). \tag{30}$$

Combining the formula for both cases, we conclude that the scalar $h_k'(\bar{\boldsymbol{c}}_k\boldsymbol{\delta}^*)$ is given by Eq. (26) with z_k from the solution of Eq. (25), and the scalar $h''(\gamma_k, \bar{\boldsymbol{c}}_k\boldsymbol{\delta}^*)$ is computed from

$$\begin{aligned} h_k''(\gamma_k, \bar{\boldsymbol{c}}_k\boldsymbol{\delta}^*) = &\frac{\cos\big(|\bar{\boldsymbol{c}}_k\boldsymbol{\delta}^*| + \mathrm{sgn}(\bar{\boldsymbol{c}}_k\boldsymbol{\delta}^*)\varphi_k\big)}{\pi - 2|\bar{\boldsymbol{c}}_k\boldsymbol{\delta}^*| - 2\mathrm{sgn}(\bar{\boldsymbol{c}}_k\boldsymbol{\delta}^*)\varphi_k} \\ &\times \big(\pi - 2|\bar{\boldsymbol{c}}_k\boldsymbol{\delta}^*| - 2\mathrm{sgn}(\bar{\boldsymbol{c}}_k\boldsymbol{\delta}^*)\varphi_k - \gamma_k\big), \end{aligned} \tag{31}$$

where the function $\mathrm{sgn}(z)$ returns the sign of its argument z. Note that both h_k' and h_k'' are chosen adaptively according to the steady-state power flow solution $\bar{\boldsymbol{c}}_k\boldsymbol{\delta}^*$, and h_k'' depends linearly on the adjustable parameter γ_k of the neighborhood $\Omega(\boldsymbol{\gamma})$. Hence, the equation (24) with our choices of h_k' and h_k'' in the adaptive sector condition provide extra degrees of freedom in constructing Lyapunov functions and certifying transient stability.

Based on the above discussion, the parametric matrices $\boldsymbol{H}'(\boldsymbol{\gamma}) \in \mathbb{R}^{2n_l \times n_l}$ and $\boldsymbol{H}''(\boldsymbol{\gamma}) \in \mathbb{R}^{2n_l \times n_l}$ of Eq. (8) in the context of power system TSA are given by

$$\boldsymbol{H}' = \begin{bmatrix} h_1'(\bar{\boldsymbol{c}}_1\boldsymbol{\delta}^*) & & \\ & \ddots & \\ & & h_{n_l}'(\bar{\boldsymbol{c}}_{n_l}\boldsymbol{\delta}^*) \\ -h_1'(-\bar{\boldsymbol{c}}_1\boldsymbol{\delta}^*) & & \\ & \ddots & \\ & & -h_{n_l}'(-\bar{\boldsymbol{c}}_{n_l}\boldsymbol{\delta}^*) \end{bmatrix}, \tag{32}$$

$$\boldsymbol{H}''(\boldsymbol{\gamma}) = \begin{bmatrix} h_1''(\gamma_1, \bar{\boldsymbol{c}}_1\boldsymbol{\delta}^*) & & \\ & \ddots & \\ & & h_{n_l}''(\gamma_k, \bar{\boldsymbol{c}}_{n_l}\boldsymbol{\delta}^*) \\ -h_1''(\gamma_1, -\bar{\boldsymbol{c}}_1\boldsymbol{\delta}^*) & & \\ & \ddots & \\ & & -h_{n_l}''(\gamma_{n_l}, -\bar{\boldsymbol{c}}_{n_l}\boldsymbol{\delta}^*) \end{bmatrix}. \tag{33}$$

Here, we suppress the notional dependence of $\boldsymbol{H}'$ and $\boldsymbol{H}''(\boldsymbol{\gamma})$ on the given equilibrium $\boldsymbol{\delta}^*$ for simplicity.

C. Solution method

Up to this point, we have instantiated the general optimization problem (14) for power system TSA by specifying matrices $\boldsymbol{A}$, $\boldsymbol{B}$, $\boldsymbol{C}$, $\boldsymbol{S}$, $\boldsymbol{H}'$, and $\boldsymbol{H}''(\boldsymbol{\gamma})$ in Eqs. (17)-(19), (21), (32), and (33), respectively. To develop an efficient solution method for this nonlinear semi-definite optimization problem, we next discuss several ways to exploit the special problem structure.

First, due to the symmetric structure of the polyhedron $\Omega(\boldsymbol{\gamma})$ in (22), we have $\underline{\boldsymbol{b}}(\boldsymbol{\gamma}) = -\boldsymbol{\gamma}$ and $\overline{\boldsymbol{b}}(\boldsymbol{\gamma}) = \boldsymbol{\gamma}$. By setting $\underline{\boldsymbol{\mu}} = \overline{\boldsymbol{\mu}} = \boldsymbol{\mu}$, the matrix inequalities (13a) and (13b) are equivalent to each other. Hence, the constraints (13a) and (13b) reduce to a single matrix inequality

$$\boldsymbol{\mu} \ge \boldsymbol{0}, \ \begin{bmatrix} \boldsymbol{P} & -\frac{1}{2}\boldsymbol{C}^{\mathrm{T}}\boldsymbol{E}_k\boldsymbol{\mu} \\ -\frac{1}{2}\boldsymbol{\mu}^{\mathrm{T}}\boldsymbol{E}_k\boldsymbol{C} & -\rho + \boldsymbol{\mu}^{\mathrm{T}}\boldsymbol{E}_k\boldsymbol{\gamma} \end{bmatrix} \ge \boldsymbol{0}, \forall 1 \le k \le n_l. \tag{34}$$

In addition, the nonlinearity in matrix inequality (9) comes from the product term $\mathrm{diag}(\boldsymbol{\lambda})\boldsymbol{H}''(\boldsymbol{\gamma})$, where $\boldsymbol{H}''(\boldsymbol{\gamma})$ is a linear matrix function in $\boldsymbol{\gamma}$, and the term $\alpha\boldsymbol{P}$. Moreover, the only nonlinearity in matrix inequality (34) lies in the term $\boldsymbol{\mu}^{\mathrm{T}}\boldsymbol{E}_k\boldsymbol{\gamma}$. Noticing the special structure of $\boldsymbol{H}''(\boldsymbol{\gamma})$ defined through Eqs. (31) and (33), we introduce three auxiliary decision vectors $\boldsymbol{\nu} \in \mathbb{R}^{n_l}$, $\boldsymbol{\kappa} \in \mathbb{R}^{n_l}$, and $\boldsymbol{\chi} \in \mathbb{R}^{n_l}$, and then let $\boldsymbol{\lambda} = [\boldsymbol{\nu}^{\mathrm{T}}\boldsymbol{\nu}^{\mathrm{T}}]^{\mathrm{T}}$, $\boldsymbol{\mu} = \mathrm{diag}(\boldsymbol{\kappa})\boldsymbol{\nu}$, and $\boldsymbol{\chi} = \mathrm{diag}(\boldsymbol{\nu})\boldsymbol{\gamma}$. Based on this reparameterization, we have

$$\mathrm{diag}(\boldsymbol{\lambda})\boldsymbol{H}''(\boldsymbol{\gamma}) = \begin{bmatrix} h_1''(\nu_1, \chi_1, \bar{\boldsymbol{c}}_1\boldsymbol{\delta}^*) & & \\ & \ddots & \\ & & h_{n_l}''(\nu_{n_l}, \chi_{n_l}, \bar{\boldsymbol{c}}_{n_l}\boldsymbol{\delta}^*) \\ -h_1''(\nu_1, \chi_1, -\bar{\boldsymbol{c}}_1\boldsymbol{\delta}^*) & & \\ & \ddots & \\ & & -h_{n_l}''(\nu_{n_l}, \chi_{n_l}, -\bar{\boldsymbol{c}}_{n_l}\boldsymbol{\delta}^*) \end{bmatrix}, \tag{35}$$

where

$$\begin{aligned} &h_k''(\nu_k, \chi_k, \bar{\boldsymbol{c}}_k\boldsymbol{\delta}^*) \\ =&\frac{\cos\big(|\bar{\boldsymbol{c}}_k\boldsymbol{\delta}^*| + \mathrm{sgn}(\bar{\boldsymbol{c}}_k\boldsymbol{\delta}^*)\varphi_k\big)}{\pi - 2|\bar{\boldsymbol{c}}_k\boldsymbol{\delta}^*| - 2\mathrm{sgn}(\bar{\boldsymbol{c}}_k\boldsymbol{\delta}^*)\varphi_k} \\ &\times \big(\pi\nu_k - 2|\bar{\boldsymbol{c}}_k\boldsymbol{\delta}^*|\nu_k - 2\mathrm{sgn}(\bar{\boldsymbol{c}}_k\boldsymbol{\delta}^*)\varphi_k\nu_k - \chi_k\big). \end{aligned}$$

In addition,

$$\boldsymbol{\mu}^{\mathrm{T}}\boldsymbol{E}_k\boldsymbol{\gamma} = \kappa_k\chi_k. \tag{36}$$

By substituting Eqs. (35) and (36) into (9) and (34), both matrix inequalities (9) and (34) become linear in $\boldsymbol{P}$, $\boldsymbol{\nu}$, $\boldsymbol{\chi}$, η, ρ given any fixed vector $\boldsymbol{\kappa}$ and scalar α. Further note that if $(\boldsymbol{P}, \boldsymbol{\nu}, \boldsymbol{\chi}, \eta, \rho)$ is a feasible solution to the optimization problem (14), any $c \cdot (\boldsymbol{P}, \boldsymbol{\nu}, \boldsymbol{\chi}, \eta, \rho)$ is also a feasible solution given any positive constant c, and the value of the objective function in (14) stays unchanged. Therefore, without loss of generality, we can set $\eta = 1$ and then the objective function in (14) also becomes a linear function in ρ.

Based on the above analysis, we employ a two-stage approach to obtain an optimal estimation of the CCT. First, given

a fixed initial guess of vector $\boldsymbol{\kappa} = \boldsymbol{\kappa}^*$, we solve the following linear SDP

$$\max_{\boldsymbol{P}\in\mathbb{S}^n,\boldsymbol{\nu}\in\mathbb{R}^{n_l},\boldsymbol{\chi}\in\mathbb{R}^{n_l},\rho\in\mathbb{R}} \ \rho, \quad \text{s.t. } (9),(34),\boldsymbol{\kappa}=\boldsymbol{\kappa}^*,\alpha=\alpha^*, \tag{37}$$

and obtain the optimal vectors $\boldsymbol{\nu}^*$ and $\boldsymbol{\chi}^*$. We then fix the values for $\boldsymbol{\nu}$ and $\boldsymbol{\chi}$ and further solve the following SDP

$$\max_{\boldsymbol{P}\in\mathbb{S}^n,\boldsymbol{\kappa}\in\mathbb{R}^{n_l},\rho\in\mathbb{R}} \ \rho, \quad \text{s.t. } (9),(34),\boldsymbol{\nu}=\boldsymbol{\nu}^*,\boldsymbol{\chi}=\boldsymbol{\chi}^*,\alpha=\alpha^*, \tag{38}$$

to obtain an improved estimation of the CCT. In principle, the above two problems (37) and (38) can be solved iteratively to further improve the CCT estimation accuracy.

D. Trajectory-exploited ALF method

Note that the aforementioned method is totally simulation-free since we use a linear function to bound the time derivative $\dot{\boldsymbol{V}}(\boldsymbol{x})$ from above along the fault-on trajectory. This upper bound is generally not tight thus bringing conservatism. If the fault-on trajectory is available, as assumed by previous energy function based direct methods, the proposed method has the flexibility to take advantage of the trajectory information to further reduce conservatism. To do this, we check every point along the trajectory until at one point $\boldsymbol{x}_F(t_{cl})$ the Lyapunov function value reaches the critical level value $V(\boldsymbol{x}_F(t_{cl})) = \rho$. The corresponding fault clearing time t_{cl} is then the estimated CCT.

In summary, the steps of trajectory information based TSA are given as follows:

Step 1: Solve two SDP problems (37) and (38) iteratively to obtain an matrix $\boldsymbol{P}$ for a given fault.

Step 2: Carry out time-domain simulation of the faulted system to acquire the fault-on trajectory $\boldsymbol{x}_F(t)$.

Step 3: Calculate the energy of points along $\boldsymbol{x}_F(t)$ until $V(\boldsymbol{x}_F(t_{cl})) = \rho$. Then, we regard t_{cl} as the estimated CCT.

As the trajectory-exploited ALF method makes full use of fault-on trajectories, it is always less conservative than the simulation-free one.

IV. Stability enhancement control

One prominent feature of the developed method is the fact that it establishes an analytic relation between the estimated CCT (or, equivalently, the transient stability certificate), the operation points, and the system control parameters in the form of matrix inequalities (9) and (34). This can enable systematic and optimization-based guidance for system operation and control design. To illustrate this point, we consider a situation where the inertia and damping parameters of generators are tunable during the transient so that they can be controlled to enhance the transient stability of the system. This scenario can be realized through virtual synchronous generators in which power-electronic converters are designed to mimic the behavior of synchronous generators and the inertia and damping are both tunable parameters. We thus seek a minimal change of inertia and damping parameters to stabilize an otherwise transiently unstable system.

Now assume that for a given fault, the fault clearing time τ_e of a system is larger than the CCT τ_D of the original system, so the system is transiently unstable under the given fault. Hence, we need to take control actions during the fault-on stage to guarantee the CCT τ_C of the controlled system is greater or equal to the fault clearing time τ_e, i.e., $\tau_C \geq \tau_e$. We denote the inertia and damping of the ith generator for the controlled system as $m_{C,i}$ and $d_{C,i}$, respectively. Then, we can mathematically formulate the stability enhancement control problem as an optimization problem:

$$\begin{aligned} \min_{m_{C,i}\geq 0, d_{C,i}\geq 0, \tau_C\in\mathbb{R}} \ & \sum_{i=1}^{n_g}(|m_{C,i}-m_i|+|d_{C,i}-d_i|), \\ \text{s.t.} \ & (9),(34),\tau_C\geq\tau_e. \end{aligned} \tag{39}$$

We now present a method to solve problem (39) to obtained the desired control strategy. Recall that if $(\boldsymbol{P},\boldsymbol{\nu},\boldsymbol{\chi},\eta,\rho)$ is a feasible solution to the optimization problem (14), any $c\cdot(\boldsymbol{P},\boldsymbol{\nu},\boldsymbol{\chi},\eta,\rho)$ is also a feasible solution given any positive constant c, and the value of the objective function in (14) stays unchanged. Hence, we can naturally set $\rho = 1$ and make η a decision variable. Then, the SDPs (37) and (38) are respectively equivalent to

$$\min_{\boldsymbol{P}\in\mathbb{S}^n,\boldsymbol{\nu}\in\mathbb{R}^{n_l},\boldsymbol{\chi}\in\mathbb{R}^{n_l},\eta\in\mathbb{R}} \ \eta, \quad \text{s.t. } (9),(34),\boldsymbol{\kappa}=\boldsymbol{\kappa}^*,\alpha=\alpha^*, \tag{40}$$

$$\min_{\boldsymbol{P}\in\mathbb{S}^n,\boldsymbol{\kappa}\in\mathbb{R}^{n_l},\eta\in\mathbb{R}} \ \eta, \quad \text{s.t. } (9),(34),\boldsymbol{\nu}=\boldsymbol{\nu}^*,\boldsymbol{\chi}=\boldsymbol{\chi}^*,\alpha=\alpha^*. \tag{41}$$

We first assign matrix $\boldsymbol{P}_C$ and multipliers $\boldsymbol{\nu}_C$ and $\boldsymbol{\chi}_C$ the same as the results obtained by solving SDPs (40) and (41). Then, as variables $m_{C,i}$ and $d_{C,i}$ appears in matrices $\boldsymbol{A}$, $\boldsymbol{B}$, and $\boldsymbol{S}$ in inequality (9), all these matrices need to be modified accordingly. We further introduce two new matrices $\boldsymbol{M}_C = \text{diag}(\frac{1}{m_{C,1}},\ldots,\frac{1}{m_{C,n_g}})$ and $\boldsymbol{D}_C = \text{diag}(\frac{d_{C,1}}{m_{C,1}},\ldots,\frac{d_{C,n_g}}{m_{C,n_g}})$. Hence, to modify $\boldsymbol{A}$, $\boldsymbol{B}$, and $\boldsymbol{S}$, we can replace matrix $\boldsymbol{M}^{-1}$ with $\boldsymbol{M}_C$ and $\boldsymbol{M}^{-1}\boldsymbol{D}$ with $\boldsymbol{D}_C$. Based on (5), inequality $\tau_C \geq \tau_e$ is equivalent to the condition

$$\eta \leq \frac{\alpha\rho}{e^{\alpha\tau_e}-1}. \tag{42}$$

Note that since we fix the matrix $\boldsymbol{P}_C$, multipliers $\boldsymbol{\nu}_C$ and $\boldsymbol{\chi}_C$, inequalities (34) are always satisfied. Hence, we can solve the following optimization problem

$$\begin{aligned} \min_{\boldsymbol{M}_C\in\mathbb{R}^{n_g},\boldsymbol{D}_C\in\mathbb{R}^{n_g},\eta\in\mathbb{R}} \ & \text{tr}(\|\boldsymbol{M}_C-\boldsymbol{M}\|^2+\|\boldsymbol{D}_C-\boldsymbol{D}\|^2), \\ \text{s.t.} \ & (9),(42),\boldsymbol{P}=\boldsymbol{P}_C,\boldsymbol{\nu}=\boldsymbol{\nu}_C,\boldsymbol{\chi}=\boldsymbol{\chi}_C, \\ & \boldsymbol{M}_C>0,\boldsymbol{D}_C>0,\alpha=\alpha^*, \end{aligned} \tag{43}$$

where $\text{tr}(\cdot)$ denotes the trace of a matrix, to obtain the inertia and damping adjustment scheme.

We now summarize the steps for stability enhancement control design:

Step 1: Given a fault and the associated clearing time τ_e.

Step 2: Solve SDPs (40) and (41) iteratively to obtain an matrix $\boldsymbol{P}_C$, and multipliers $\boldsymbol{\nu}_C$ and $\boldsymbol{\chi}_C$.

Step 3: Solve problem (43) to obtain the inertia and damping adjustment scheme for generators.

Note that constraint (42) is related to the estimated CCT τ_C of the controlled system. Due to the inherent conservatism of the direct method, if $\tau_C \geq \tau_e$, the exact CCT of the controlled

TABLE I
OPTIMAL PARAMETERS AND CCTS OF TWO ALF METHODS UNDER DIFFERENT SEPS WITH THE SAME INITIAL VALUE $\alpha = 1$ AND $\kappa = 1$ COMPARED WITH THE CCTS OBTAINED BY THE METHOD IN [10], THE ENERGY FUNCTION METHOD, AND TIME-DOMAIN SIMULATION

δ^* (rad)	γ	h'	$h''(\gamma)$	CCT (s) Simulation-free	CCT (s) Trajectory-exploited	CCT (s) [10]	CCT (s) Energy function	CCT (s) Time-domain
-0.253	2.118	0.992	0.190	1.422	4.790	0.824	7.439	8.125
0.253	2.118	0.992	0.190	1.422	4.790	0.824	7.439	8.125
0.524	1.816	0.966	0.115	1.131	2.448	0.541	2.776	3.310
0.848	1.446	0.913	0.000	0.751	1.308	0.248	0.911	1.600
1.120	0.902	0.852	0.000	0.387	0.556	0.097	0.182	0.825
1.430	0.283	0.768	0.000	0.024	0.100	0.010	0.020	0.225

system is definitely greater than τ_e. Hence, the controlled system is guaranteed to meet the stability requirement.

V. NUMERICAL RESULTS

Here, we demonstrate the effectiveness and performance of the proposed TSA method on several IEEE benchmark systems. The generators are modeled with the second-order classical model in which the excitation voltage is assumed to stay constant during the transient. The loads are modeled as first-order systems. The numerical results of the proposed method are obtained by solving the two SDPs (37) and (38) only once, and comparative studies are conducted between the proposed ALF method and the LLF method recently introduced in [10]. Both methods are implemented in MATLAB with the modeling tool YALMIP and optimization solver Mosek.

A. Single-machine-infinite-bus (SMIB) system

For an illustrative example, we first analyze the working mechanism and performance of the proposed method on the SMIB system described by

$$m\ddot{\delta} + d\dot{\delta} + \sigma\sin(\delta) - p = 0, \tag{44}$$

where m, d, σ, and p are inertia, damping, coupling strength, and power mismatch, respectively. The SEP of the system is given by $[\delta^*; 0]$ where $\delta^* = \arcsin(p/\sigma)$. In this system, the parameters $m = 0.1$, $d = 0.15$, and $\sigma = 0.2$.

By choosing different power mismatch parameters p, the system can operate at different SEPs. Table I compares the estimated CCTs by the proposed methods with those by the method in [10], the energy function method, and time-domain simulation, under four different SEPs. It is shown that the proposed method increases the CCT estimation by 1.97 times on average compared with the previous method, indicating a significant reduction in conservatism. Such improvement largely comes from the novel techniques proposed in this paper, including the non-uniform bound for the time derivative of the Lyapunov function (3), the adjustable neighborhoods (12), and the adaptive sector conditions (8). As shown in columns 2–4 of TableI, the neighborhood parameter γ and the slopes of the sector conditions h' and h'' are adaptive to the change of the SEPs. Fig. 3a–3c visualize the neighborhood and sector conditions under different SEPs. Due to the adaptiveness

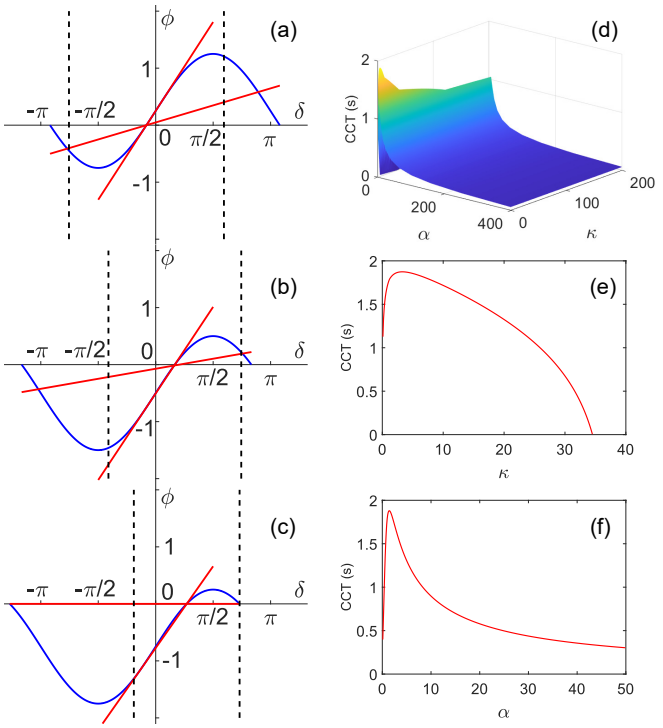

Fig. 3. Numerical results of the proposed method on the SMIB system. (a)–(c) The adaptive sector bounds for the nonlinear term at different SEPs $\delta^* = -0.253$, $\delta^* = 0.524$, and $\delta^* = 0.848$ with $\alpha = 1$ and $\kappa = 1$. The two vertical dashed lines indicate the boundary of $\Omega(\gamma)$. (d) The mesh plot of the estimated CCT with different initial values of $\alpha \in [10^{-3}, 10^3]$ and $\kappa \in [0, 200]$. (e) The dependence of the estimated CCT on κ with fixed $\alpha = 1.585$. (f) The dependence of the estimated CCT on α with $\kappa = 3.300$.

of neighborhood $\Omega(\gamma)$ and the sector conditions, the proposed method gains extra degrees of freedom to construct superior Lyapunov functions that enables tighter CCT estimation.

Next, we reveal the dependence of the estimated CCTs on parameters α and κ of the proposed algorithm, as illustrated in Fig. 3d–3f. For this purpose, the power mismatch is set to $p = 0.1$ and hence the SEP is $[\pi/6; 0]$. Fig. 3d illustrates the CCT estimation results using different parameters $\alpha \in [10^{-3}, 10^3]$ and $\kappa \in [0, 200]$. It is shown that the estimated CCT reaches its peak which is 1.87 s when $\alpha = 1.585$ and $\kappa = 3.300$. Note that the proposed method is still conservative (the exact CCT from the time-domain simulation is 3.31 s), but the conservatism of the proposed method is much lower compared

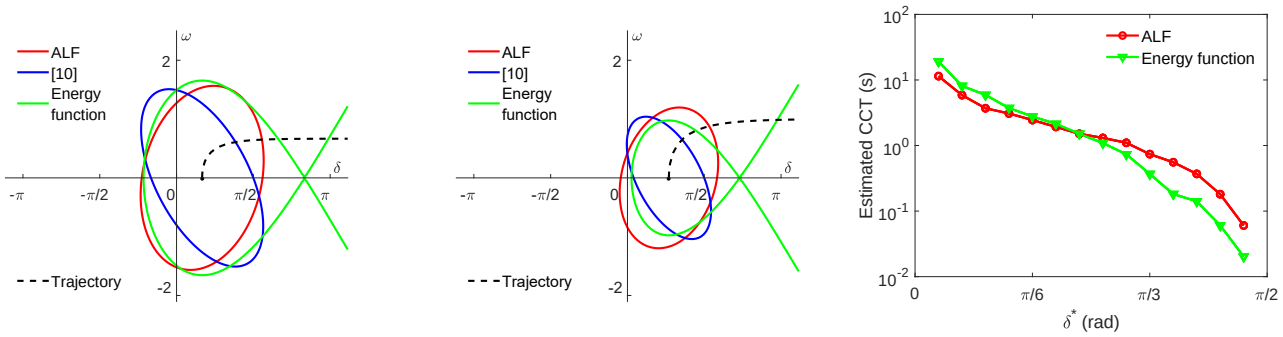

(a) (b) (c)

Fig. 4. Comparison of the estimated stability boundary based on the proposed ALF method, the LLF method [10], and the energy function method when (a) $\delta^* = 0.524$, and (b) $\delta^* = 0.848$. Sub-figure (c) presents the comparison of the CCT estimation results (in logarithmic scale) for different δ^* by using the trajectory-exploited ALF method and energy function method.

with the existing LLF methods (0.54 s in [10] and 1.06 s in [26]). Moreover, it can be concluded that, as either α or κ increases, the estimated CCT becomes almost independent to the variation of the other parameter. On the other hand, when α (or κ) is fixed at a relatively small value, the estimated CCT is sensitive to the value of κ (or α). This is clearly demonstrated in Fig. 3e and 3f which are cross-sections of Fig. 3d at the point where the largest CCT estimation is attained. According to our experiences, to obtain reasonably tight CCT estimation, the initial value of parameter α can be chosen in the interval $[1, 10]$, and the initial choice of parameter κ should not exceed 10 and should be smaller when the system scale increases.

Going further, we use the actual fault-on trajectory information to amend $\dot{\boldsymbol{V}}(\boldsymbol{x})$ along the trajectory. As $\dot{\boldsymbol{V}}(\boldsymbol{x})$ is exactly known, the trajectory-exploited ALF is less conservative than the simulation-free one. We make a comparison between the trajectory-exploited ALF method and the classical energy function method as the latter also exploits fault-on trajectory information so the comparison is fair and meaningful. Columns 6 and 8 in Table I lists the numerical results corresponding to the method discussed in Section-III-D and the energy function method using controlling UEP [1]. It is shown in Table I and Fig. 4c that, the proposed method is initially more conservative than the energy function based method when the operation equilibrium is far away from the static limit. However, as the system loading further increases, the proposed ALF method actually becomes less conservative than the controlling UEP based global energy function method at a relatively higher load level when the transient stability problem is more relevant. Fig. 4a–4b visualize the stability boundary of three different approaches under different SEPs. For the case of $\delta^* = 0.524$ (Fig. 4a), the fault-on trajectory (black dashed curve) intersects the ALF-based stability boundary before going through the energy function based boundary. Hence, the ALF-based CCT estimation is relatively small. This phenomenon coincides with the numerical results shown in Table I. On the contrary, in Fig. 4b, i.e., $\delta^* = 0.848$, the fault-on trajectory intersects the ALF-based boundary after the energy function based one, resulting in a larger CCT estimation by using the ALF method. To reveal the trend of the CCT estimation for different SEPs, Fig. 4c illustrates the comparison of the CCT estimation results (in logarithmic scale) for different δ^* by using trajectory-exploited ALF method and energy function method. It is clear that the proposed ALF method is a little conservative when the system operates far away from the boundary $\pi/2$. However, for systems operating in stressful conditions, e.g., the operating point nears $\pi/2$, the ALF method has better estimation results.

B. IEEE benchmark systems

To demonstrate the effectiveness of the proposed TSA method for multi-machine systems, extensive numerical studies are carried out on three benchmark systems, i.e., the New England 10-generator 39-bus system (NE 39-bus system) [35], the IEEE 68-bus system [36], and the IEEE 118-bus system [37]. For each test system, the damping coefficients d_i are set uniformly to be $\min\{m_i\}$ with the inertia parameters m_i directly available from the dataset. In the implementation of the proposed method, we set the initial values of parameters $\alpha = 10$ and $\kappa = 0.1$. The faults considered in this study are the tripping of transmission lines which are then automatically re-closed by protection systems. When the reclosure is successful, the post-fault SEP of the system is identical to the pre-fault SEP. In this setting, the CCT for each line is the maximum amount of time between the tripping and re-closing of the transmission line such that the system remains stable.

Implementing both the proposed simulation-free method and the previous method [10] to estimate the CCT corresponding to each line, we conduct comparative research for the two methods on the three benchmark systems. The results are demonstrated in Fig. 5. For the NE 39-bus system, as illustrated in Fig. 5a, our method has improved the CCT estimation by about 21 times on average compared with the results from the previous method [10]. Among all the 46 lines in this system, the CCT for line 14 (between buses 7 and 8) shows the least improvement of about 2.84 times, whereas the CCT for line 46 (between buses 31 and 6) has the largest improvement of about 97 times. For the IEEE 68-bus system, the proposed method increases the CCT estimation by about 26 times on average, as shown in Fig.5b. Note that, under the current

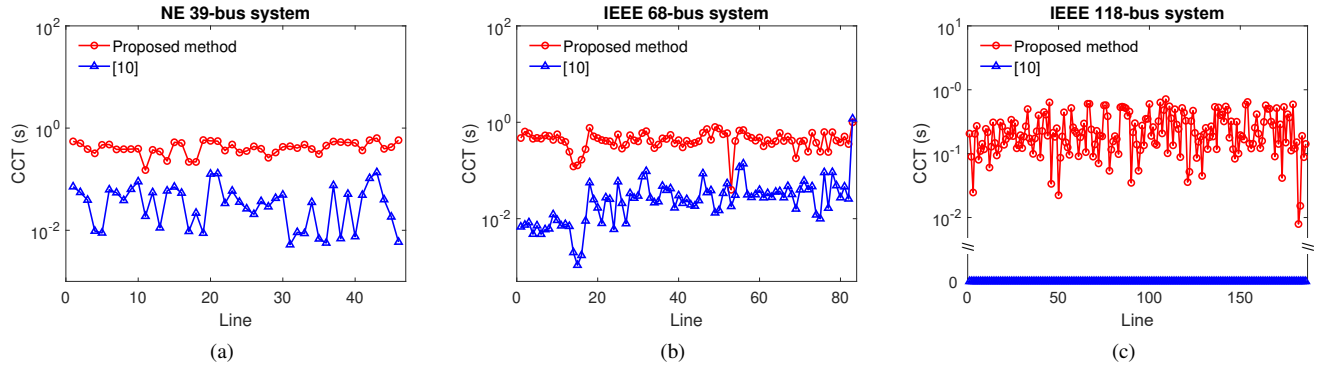

(a) (b) (c)

Fig. 5. Comparison results (in logarithmic scale) of the estimated CCT based on the proposed simulation-free ALF method and the LLF method [10] for each line on the (a) NE 39-bus, (b) IEEE 68-bus, and (c) IEEE 118-bus systems.

TABLE II
COMPARISONS OF CCTS OBTAINED BY THE METHOD IN [10], SIMULATION-FREE ALF METHOD, TRAJECTORY-EXPLOITED ALF METHOD, AND THE TIME-DOMAIN SIMULATION UNDER LINE TRIPPING FAULTS (UNIT: SECOND)

System	Line	[10]	Proposed simulation-free	Proposed trajectory-exploited	Time-domain simulation
39-bus	4	0.010	0.313	2.173	6.152
	38	0.007	0.518	1.328	16.234
	46	0.006	0.583	1.643	15.201
68-bus	11	0.007	0.425	1.000	9.505
	27	0.008	0.335	0.403	6.512
	53	0.018	0.039	0.381	1.656
118-bus	3	-	0.025	0.100	0.803
	50	-	0.023	0.063	0.942
	117	-	0.038	0.060	0.371

algorithm parameter $\alpha = 10$, there is one line (i.e., line 83) whose corresponding estimated CCT by our method is slightly lower than that from the previous method [10]. However, if we decrease the parameter α from 10 to 1, we obtain the estimated CCT of the proposed method is 5.77 s, which is about 4 times higher than that of method in [10] (1.18 s). For the IEEE 118-bus system, the proposed method still works well and provide an estimation of the CCT corresponding to each transmission line. In stark contrast, the method in [10] fails to find feasible solutions for the problem of constructing Lyapunov functions, resulting in the estimated CCTs being zeros for all transmission lines. The results are visualized in Fig. 5c. From the above comparative studies, relative to the previous LLF method [10], the proposed ALF method significantly reduces the conservatism of stability certificate and CCT estimation and also broaden the applicability of LLF methods to larger systems that were otherwise intractable.

Admittedly, the numerical scalability of the proposed ALF method still poses limitations on its practical applicability. In particular, the average computation time to obtain the CCT estimations using a Intel Xeon E7-8867v4 processor are about 1 minute, 20 minutes, and 12 hours for the 39-, 68-, and 118-bus systems, respectively. The major computational burden lies in solving the SDPs whose sizes increase with the number of buses and lines in the network. Nevertheless, the solid theoretical foundation and reduced conservatism of the proposed ALF indicates that this general framework is promising and worth for more systematic and application-oriented research. It can be expected that, by further exploiting special problem structures, e.g., sparsity, locality, and symmetry, the computational burden can be significantly reduced, which could lead to more practical variant of the proposed method.

To make a comprehensive comparison of the results obtained via different approaches, we present some quantitative results in Table II. It is obvious that the proposed simulation-free approach is less conservative compared to the method in [10] due to three major techniques introduced in this paper: the adaptive sector bound for nonlinearities, the non-uniform upper bound for the time derivative of the Lyapunov function along the fault-on trajectory, and the co-optimization of the construction of Lyapunov functions and the lower bound estimation of CCT. The simulation-free ALF method does not assume the knowledge of fault-on trajectory information. If the fault-on trajectory is available, the value of the Lyapunov function along the trajectory can be exactly calculated. Then, by locating the time when the value of the Lyapunov function is equal to the critical value ρ, a less conservative trajectory-exploited estimation of the CCT can be obtained as shown in the fifth column in Table II.

It is worth noting that the proposed ALF method can also be used to analyze the stability of a system suffering a short-

TABLE III
COMPARISONS OF CCTS OBTAINED BY THE METHOD IN [10], SIMULATION-FREE ALF METHOD, TRAJECTORY-EXPLOITED ALF METHOD, AND THE TIME-DOMAIN SIMULATION UNDER SHORT CIRCUIT FAULTS (UNIT: SECOND)

System	Bus	[10]	Proposed simulation-free	Proposed trajectory-exploited	Time-domain simulation
39-bus	12	0.002	0.087	0.093	0.482
	20	0.002	0.223	0.253	0.850
	28	0.002	0.108	0.119	0.694
68-bus	12	0.001	0.053	0.070	0.444
	39	0.001	0.046	0.060	0.463
	48	0.001	0.084	0.100	0.721
118-bus	20	-	9e-4	0.003	0.030
	45	-	7e-4	0.003	0.020
	64	-	0.008	0.008	0.032

circuit fault. In this paper, we use a large load $P_S = 10^2$ p.u. connecting to a bus i to simulate the short-circuit fault. To consider short-circuit faults in the ALF method, we need to modify the matrix $\boldsymbol{S}$ to be a column vector $\tilde{\boldsymbol{S}}$ of dimension $(n_b + n_g) \times 1$ which can be obtained via

$$\tilde{\boldsymbol{S}} = \begin{bmatrix} \boldsymbol{R}^{-1} & \mathbf{0}_{n_c \times n_g} \\ \mathbf{0}_{n_g \times n_c} & \mathbf{0}_{n_g \times n_g} \\ \mathbf{0}_{n_g \times n_c} & \boldsymbol{M}^{-1} \end{bmatrix} \cdot \tilde{\boldsymbol{E}}_i \cdot \mathbb{1} \cdot P_S, \quad i = 1, \cdots, n_b,$$

where $\tilde{\boldsymbol{E}}_i$ is a $(n_b + n_g)$-dimension square matrix whose (i,i)th element is 1 and all other elements are zeros; $\mathbb{1}$ is a column vector of proper dimension with all elements being 1. In addition, the third column and the third row in LMI (9) should be modified to the appropriate dimension. After these modifications, by solving SDPs (37) and (38) iteratively, we can obtain the TSA results of short-circuit faults for different benchmark systems. The results of the NE 39-bus, IEEE 68-bus, and IEEE 118-bus systems are listed in Table III. It can be found that the estimation of the CCT obtained by the proposed ALF method are less conservative than those from the method developed in [10]. In addition, the use of fault-on trajectory information helps further reduce conservatism. Admittedly, all the direct methods suffer from a certain degree of conservatism so the CCT estimations provided by direct methods are always conservative compared with the exact CCT given by time-domain simulation.

C. Stability enhancement control

Here, we demonstrate the effectiveness of the control design approach proposed in Section-IV using the three IEEE benchmark systems. Fig. 6 shows the comparative time-domain simulations of NE 39-bus, IEEE 68-bus, and IEEE 118-bus systems without (Fig. 6 (a), (c), (e)) and with (Fig. 6 (b), (d), (f)) the obtained control strategies. Fig. 6a–6b demonstrates the angular difference of NE 39-bus system under a short-circuit fault at bus 12. From Table III, the system is judged to be unstable if the fault is cleared after 0.5 seconds, which is visualized in the sub-figure Fig. 6a. By implementing the obtained control strategy during the fault-on stage, the system becomes stable given the same fault clearing time 0.5 seconds (as shown in the sub-figure Fig. 6b). Similar results are observed for short-circuit fault at bus 39 in IEEE 68-bus system. The original system is unstable if the fault clearing time is larger than 0.5 seconds (as shown in Fig. 6c). After controlling the system parameter during the fault-on stage, the system maintains stability under the same fault clearing time (as shown in Fig. 6d). Similarly, for the IEEE 118-bus system, a short-circuit fault occurs at bus 45, and the original system is unstable if the fault persists for 0.02 seconds (as shown in Fig. 6e). By taking the obtained control actions, the system can withstand the fault for 0.02 seconds without losing stability (as shown in Fig. 6f).

VI. DISCUSSION

This paper proposes an ALF method to systematically perform TSA with reduced conservatism. An adaptive sector condition in an adjustable neighborhood of the post-fault SEP is proposed to bound the nonlinearities of the power system model, which provides extra degrees of freedom for the construction of a Lyapunov function. An improved simulation-free bounding technique is introduced to provide tighter estimation for the time derivative of the Lyapunov function during the fault-on dynamics. By integrating above novel ideas, the parameters in the candidate Lyapunov functions along with those in the sector conditions are co-optimized to obtain the tightest possible estimation of the CCT. Preliminary numerical results show that the proposed adaptive Lyapunov function approach reduces the conservatism in CCT estimation by about one order of magnitude compared with the existing methods using local Lyapunov functions.

Admittedly, the proposed method involves solving computationally expensive SDPs and thus is currently not suitable for online transient stability assessment because solving large-scale SDPs in real-time is still not feasible for the state-of-the-art solvers. To enable online TSA, some computations have to be done offline and problem structures need to be further exploited in numerical methods to accelerate calculations. However, the rigorous theoretical foundation and the reduced conservatism of the proposed method indicate that it is promising for future research and industrial applications. To make the proposed basic framework of ALF method applicable to TSA for practical power systems, extensions of this work that

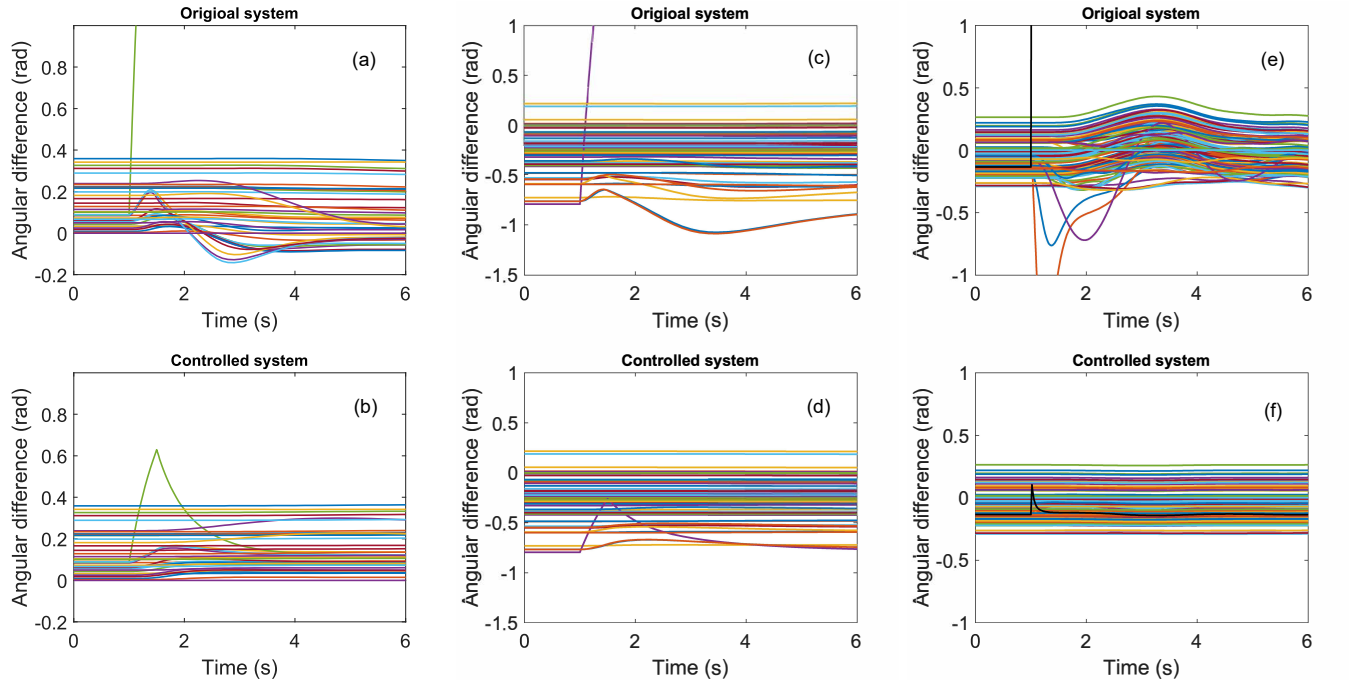

Fig. 6. Stability enhancement control results of the proposed ALF method. In which (a) and (b) illustrate the stability of the NE 39-bus system before and after control actions, (c) and (d) illustrate the stability of the IEEE 68-bus system before and after control actions, while (e) and (f) illustrate the stability of the IEEE 118-bus system before and after control actions.

warrant further research include 1) the consideration of more detailed power system models and renewable generation units based on differential-algebraic equations [38], 2) systematic approaches to treat general nonlinearities in power system models using robust [39] or polynomial [40] optimization methods, 3) the development of sparsity-exploiting techniques in solving transient stability certificate to improve numerical scalability [41], and 4) the construction of more general forms of Lyapunov functions that exploits special structures of detailed power system models.

More importantly, going beyond solving the *analysis* problems of power system transient stability, this general framework of ALF method also has great potential for providing systematic solutions to the *synthesis* problems. The proposed ALF method establishes an analytic relationship between transient stability certificate, operation points, and control parameters in the form of matrix inequalities (9) and (13), which can provide systematic and optimization-based guidance for operation scheduling and control design. We have exemplified how the proposed framework can be used to design virtual inertia and damping controllers to stabilize a previously unstable system under a given fault. A similar idea can be applied to the scheduling of operation points, which would create a new paradigm for transient stability constrained OPF to be explored in our future research.

REFERENCES

[1] H. D. Chiang, *Direct Methods for Stability Analysis of Electric Power Systems*, USA, NJ, Hoboken:Wiley, 2011.

[2] P. M. Anderson and A. A. Fouad, *Power Systems Control and Stability*, ser. IEEE Press Power Engineering Series, 2nd ed. New York, NY, USA: Wiley, 2003.

[3] P. Kundur, *Power Systems Stability*, New York, NY, USA: McGraw-Hill, 1994.

[4] A. R. Sobbouhia and A. Vahedi, "Transient stability prediction of power system: a review on methods, classification and considerations," *Elect. Power Syst. Res.,* vol. 190, Jan. 2021.

[5] M. Pertl, T. Weckesser, M. Rezkalla and M. Marinelli, "Transient stability improvement: a review and comparison of conventional and renewable-based techniques for preventive and emergency control," *Electr Eng.,* vol. 100, no. 3, pp. 1701–1718, Sep. 2018.

[6] I. Nagel, L. Fabre, M. Pastre, François Krummenacher, Rachid Cherkaoui and Maher Kayal. "High-speed power system transient stability simulation using highly dedicated hardware," *IEEE Trans. Power Syst.,* vol. 28, no. 4, pp. 4218-4227, Nov. 2013.

[7] M. A. Tomim, J. R. Martí and J. A. Passos Filho, "Parallel transient stability simulation based on multi-area Thévenin equivalents," *IEEE Trans. Smart Grid.,* vol. 8, no. 3, pp. 1366-1377, May 2017.

[8] S. Zadkhast, J. Jatskevich and E. Vaahedi, "A multi-decomposition approach for accelerated time-Domain simulation of transient stability problems," *IEEE Trans. Power Syst.,* vol. 30, no. 5, pp. 2301-2311, Sept. 2015.

[9] Y. Liu and Q. Jiang, "Two-stage parallel waveform relaxation method for large-scale power system transient stability simulation," *IEEE Trans. Power Syst.,* vol. 31, no. 1, pp. 153-162, Jan. 2016.

[10] T. L. Vu and K. Turitsyn, "A framework for robust assessment of power grid stability and resiliency," *IEEE Trans. Autom. Control.,* no.3, pp. 1165-1177, March 2017.

[11] T. Odun-Ayo and M. L. Crow, "Structure-Preserved Power System Transient Stability Using Stochastic Energy Functions," *IEEE Trans. Power Syst.,* vol. 27, no. 3, pp. 1450-1458, Aug. 2012.

[12] H. D. Chiang, C.C. Chu and G. Cauley, "Direct stability analysis of electric power systems using energy functions: theory, applications, and perspective," *Proc. IEEE Proc. IRE*.,* vol. 83, no. 11, pp. 1497-1529, Nov. 1995.

[13] H. D. Chiang, F. F. Wu and P. P. Varaiya, "A BCU method for direct analysis of power system transient stability," *IEEE Trans. Power Syst.,* vol. 9, no. 3, pp. 1194-1208, Aug. 1994.

[14] Y. Xue, T. Van Custem and M. Ribbens-Pavella, "Extended equal area criterion justifications, generalizations, applications," *IEEE Trans. Power Syst.,* vol. 4, no. 1, pp. 44-52, Feb. 1989.

[15] Y. Zhang et al., "Hybrid extended equal-area criterion for fast transient stability assessment with detailed power system models", *Proceedings of IFAC Control of Power Plants and Power Systems,* pp. 49-54, 1995.

[16] K.W. Chan, Q. Zhou and T.S. Chung, "Transient stability margin assessment for large power system using time domain simulation based on hybrid extended equal area criterion method", *Proc. Int. Conf. Adv. Power Syst. Control Oper. Manage.*, pp. 405-409, 2000.

[17] A. Bahmanyar, D. Ernst, Y. Vanaubel, Q. Gemine, C. Pache and P. Panciatici. "Extended equal area criterion revisited: A direct method for fast transient stability analysis", *Energies*, vol. 14, no. 21, pp. 7259, Nov. 2021.

[18] Y. Li, S. Huang, H. Li and J. Zhang, "Application of phase sequence exchange in emergency control of a multi-machine system", *Int. J. Elect. Power Energy Syst.,* vol. 121, Oct. 2020.

[19] Y. Xue et al., "An efficient and robust case sorting algorithm for transient stability assessment", *Proc. IEEE Power Energy Soc. Gen. Meeting,* pp. 1-5, Jul. 2015.

[20] H. Yuan and Y. Xu, "Preventive-corrective coordinated transient stability dispatch of power systems with uncertain wind power", *EEE Trans. Power Syst.,* vol. 35, no. 5, pp. 3616-3626, Sep. 2020.

[21] P. Bhui and N. Senroy, "Real-time prediction and control of transient stability using transient energy function," *IEEE Trans. Power Syst.,* vol. 32, no. 2, pp. 923–934, Mar. 2017.

[22] F. Al Hasnain, A. Sahami and S. Kamalasadan, "An online wide-area direct coordinated control architecture for power grid transient stability enhancement based on subspace identification", *IEEE Trans. Ind. Appl.,* vol. 57, no. 3, pp. 2896-2907, May/Jun. 2021.

[23] P. Ju, H. Li, C. Gan, Y. Liu, Y. Yu and Y. Liu, "Analytical assessment for transient stability under stochastic continuous disturbances", *IEEE Trans. Power Syst.,* vol. 33, no. 2, pp. 2004-2014, Mar. 2018.

[24] D. Rimorov, X. Wang, I. Kamwa and G. Joos, "An approach to constructing analytical energy function for synchronous generator models with subtransient dynamics", *IEEE Trans. Power Syst.,* vol. 33, no. 6, pp. 5958-5967, Nov. 2018.

[25] T. L. Vu and K. Turitsyn, "Lyapunov functions family approach to transient stability assessment," *IEEE Trans. Power Syst.,* vol. 31, no. 2, pp. 1269-1277, March. 2016.

[26] T. L. Vu, S. M. Al Araifi, M. S. El Moursi and K. Turitsyn, "Toward simulation-free estimation of critical clearing time," *IEEE Trans. Power Syst.,* vol. 31, no. 6, pp. 4722-4731, Nov. 2016.

[27] S. M. Al Araifi, M. S. E. Moursi and S. M. Djouadi, "Individual functions method for power system transient stability assessment," *IEEE Trans. Power Syst.,* vol. 35, no. 2, pp. 1264-1273, March 2020.

[28] C. Mishra, A. Pal, J. S. Thorp and V. A. Centeno, "Transient stability assessment of prone-to-trip renewable generation rich power systems using Lyapunov's direct method", *IEEE Trans. Sustain. Energy.,* vol. 10, no. 3, pp. 1523-1533, Jul. 2019.

[29] S. Boyd, L. El Ghaoui, E. Feron and V. Balakrishnan. *Linear matrix inequalities in system and control theory*. Society for industrial and applied mathematics, Philadelphia, PA, USA: SIAM, 1994.

[30] L. Aolaritei, D. Lee, T. L. Vu and K. Turitsyn, "A robustness measure of transient stability under operational constraints in power systems," *IEEE Contr. Syst. Lett.,* vol. 2, no. 4, pp. 803-808, Oct. 2018

[31] W. M. Haddad and V. Chellaboina, *Nonlinear Dynamical Systems and Control: A Lyapunov-Based Approach,* Princeton, NJ, USA:Princeton Univ. Press, 2008.

[32] A. R. Bergen and D. J. Hill, "A structure preserving model for power system stability analysis," *IEEE Trans. Power App. Syst*.,* vol. PAS-100, no. 1, pp. 25-35, Jan. 1981.

[33] F. Dorfler, M. Chertkov and F. Bullo, "Synchronization in complex oscillator networks and smart grids," *Proc. National Acad. Sci. USA,* vol. 110, no. 6, pp. 2005–2010, 2013.

[34] A. Ben-Tal and A. Nemirovski, "Lectures on modern convex optimization." 2019. [online]. Available: https://www2.isye.gatech.edu/ nemirovs/LMCO_LN.pdf

[35] C. Canizares et al., "Benchmark systems for small signal stability analysis and control," 2015. [online]. Available: https://resourcecenter.ieee-pes.org/publications/technical-reports/PESTR18.html.

[36] A. K. Singh and B. C. Pal, "IEEE PES task force on benchmark systems for stability controls—Report on the 68-bus 16-machine 5-area system", 2013.

[37] R. D. Zimmerman, C. E. Murillo-Sanchez and R. J. Thomas, "MATPOWER: steady-state operations, planning and analysis tools for power systems research and education," *IEEE Trans. Power Syst.,* vol. 26, no. 1, pp. 12–19, Feb. 2011.

[38] P. Di Franco, G. Scarciotti and A. Astolfi, "Stability of nonlinear differential-algebraic systems via additive identity," *IEEE/CAA J. Automatica Sinica* vol. 7, no. 4, pp. 929-941, July 2020.

[39] G. Blekherman and P.A. Parrilo and R.R. Thomas, *Robust optimization*, Princeton university press, 2009.

[40] G. Blekherman and P.A. Parrilo and R.R. Thomas, *Semidefinite optimization and convex algebraic geometry*, SIAM, 2012.

[41] L. Vandenberghe and M. S. Andersen, "Chordal graphs and semidefinite optimization", *Found. Trends Optim.*, vol. 1, no. 4, pp. 241-433, 2015.